Available on CMS information server

CMS AN-2007/039

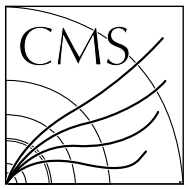

The Compact Muon Solenoid Experiment

Analysis Note

The content of this note is intended for CMS internal use and distribution only

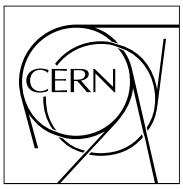

12 November 2007

CMS Search Plans and Sensitivity to New Physics using Dijets

Marco Cardaci and Benjamin Bollen

Universiteit Antwerpen, Antwerp, Belgium

Selda Esen

Brown University, Providence, RI, USA

Manoj K. Jha

University of Delhi, India and INFN, Bologna, Italy

Frank Chlebana, Robert M. Harris, Konstantinos Kousouris and David Mason

Fermilab, Batavia, IL, USA

Marek Zielinski

University of Rochester, Rochester, NY, USA

Anwar Bhatti

Rockefeller University, New York, NY, USA

Abstract

We present CMS plans to search for physics beyond the standard model using dijets. We study the jet trigger, jet cleanup, jet response versus η, optimization of η cuts, and the dijet mass resolution. Estimates are presented for both the QCD background and signals of new physics with a focus on the integrated luminosities 10 pb^{-1}, 100 pb^{-1}, and 1 fb^{-1} expected early in LHC running. The inclusive cross section as a function of jet p_T is a first simple measure of QCD dijets which is sensitive to a 3 TeV contact interaction with only 10 pb^{-1}. With the dijet mass distribution we expect to be able to convincingly observe dijet resonances with large cross sections, such as a 2 TeV excited quark which produces a 13σ signal with 100 pb^{-1}. With the dijet ratio, a simple angular measurement, we expect to be able to discover a contact interaction scale Λ^+ of 4, 7 and 10 TeV for integrated luminosities of 10 pb^{-1}, 100 pb^{-1}, and 1 fb^{-1} respectively. Using the dijet ratio we can discover or confirm a dijet resonance, and eventually measure its spin. With 100 pb^{-1} a 2 TeV resonance with the production rate of an excited quark produces a convincing signal in the dijet ratio.

Contents

1 Introduction

In this note we summarize the CMS work since the physics TDR [1] on searches for new physics using dijets. Some of the work on dijet mass and the dijet ratio is available in separate analysis notes [2, 3] which provide further detail by the original authors. Here we present the status of all ongoing CMS dijet analysis that is directed towards new physics. We hope to present them in a coherent order so the reader can see their commonality and the breadth of the new physics they probe.

This note presents our current plans for how we will analyze the first available data samples. The analysis strategies are intentionally kept simple. We anticipate that even the most simple plans will in the beginning have challenging detector and analysis issues to confront. The physics TDR presented a good base plan. Here we try to clarify our plans in areas not discussed by the physics TDR.

This note presents estimates of our sensitivity to new physics. Since our focus is the first available data samples, these estimates are for integrated luminosities of 10 pb^{-1}, 100 pb^{-1} and 1 fb^{-1}. The physics TDR presented a more complete analysis of sensitivity to new physics for integrated luminosities between 100 pb^{-1} and 10 fb^{-1}. Here we have concentrated instead on improving the analysis cuts, for example the η cuts, and on introducing new analysis strategies, for example inclusive jet p_T and the dijet ratio search in dijet resonances. Where comparable, our sensitivity results are all compatible with those presented in the physics TDR.

1.1 QCD Dijets and Inclusive Jets

Inclusive dijet production ($pp \rightarrow 2$ jets + anything) is the dominant LHC process. To lowest order it arises from the $2 \rightarrow 2$ QCD scattering of partons (quarks, antiquarks, and gluons) in which there are only partons in the initial, intermediate and final states. Inclusive jets and dijets both originate from this scattering. The distinction between inclusive jets and dijets is only in a different way of measuring the same process. For inclusive jets we count the number of jets inside an η cut as a function of jet p_T. For dijets we select events in which the two highest p_T jets, the leading jets, are each inside the η cut and count events as a function of the dijet mass. In both cases we are dealing with an inclusive process with a QCD rate dominated by the $2 \rightarrow 2$ QCD scattering of partons. For a common choice of η cut, the events selected by the dijet analysis will be a subset of the events selected by the inclusive jet analysis, but the number of events in the two analyses coming from QCD is expected to be close at high p_T.

1.2 Signals of New Physics

Dijet resonances and contact interactions are the two major signals of new physics with dijets. Dijet resonances produce compelling signals of a new particle at a mass M, but require that the incoming parton-parton collision energy be close to that mass which must be kinematically accessible. Contact interactions produce more ambiguous signals but come from an energy scale of new physics, Λ, which can be significantly larger than the available collision energy.

1.2.1 Dijet Resonances

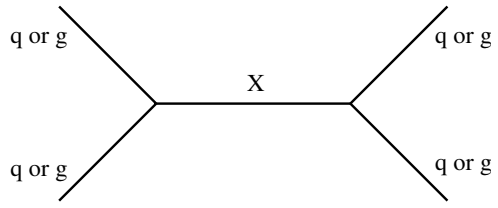

Figure 1: Feynman diagram for a dijet resonance. The initial state and final state both contain two partons (quarks, antiquarks or gluons) and the intermediate state contains an s-channel resonance X.

We search for processes producing narrow resonances, X, decaying to dijets: $pp \rightarrow X \rightarrow 2$ jets, inclusive, as pictured in Figure 1. Our experimental motivation is that LHC is a parton-parton collider, and resonances made from partons must decay to the same partons giving two jets in the final state. The theoretical motivation is broad, since there are many models that predict narrow dijet resonances. Here we will discuss very briefly the subset of the physics TDR models [4] that we investigate in this analysis, with an emphasis on the η cut optimization and

the angular distribution aspects explored using the dijet ratio. Table 1 lists the spin, color and cross section for the models we consider.

			Cross Section (pb)					
			M=0.7 TeV		M=2.0 TeV		M=5.0 TeV	
Model	J	Color	$\|\eta\| < 1$	$\|\eta\| < 1.3$	$\|\eta\| < 1$	$\|\eta\| < 1.3$	$\|\eta\| < 1$	$\|\eta\| < 1.3$
q*	1/2	Triplet	7.95×10^{2}	1.27×10^{3}	9.01	1.36×10^{1}	1.82×10^{-2}	2.30×10^{-2}
A,C	1	Octet	3.22×10^{2}	5.21×10^{2}	5.79	8.82	1.55×10^{-2}	2.04×10^{-2}
D	0	Triplet	8.11×10^{1}	1.26×10^{2}	4.20	5.97	4.65×10^{-2}	5.75×10^{-2}
G	2	Singlet	3.57×10^{1}	5.47×10^{1}	1.83×10^{-1}	2.60×10^{-1}	2.64×10^{-4}	3.19×10^{-4}
W'	1	Singlet	1.46×10^{1}	2.37×10^{1}	3.49×10^{-1}	5.31×10^{-1}	8.72×10^{-4}	1.17×10^{-3}
Z'	1	Singlet	8.86	1.44×10^{1}	1.81×10^{-1}	2.77×10^{-1}	5.50×10^{-4}	7.26×10^{-4}

Table 1: We list for each resonance model the spin (J), the color multiplet, and the lowest order cross section [4] times branching ratio times acceptance for dijet resonances with two different values of η cut for three different resonance masses. The models are excited quarks (q^*), axigluons (A), colorons (C), E_6 diquarks (D), Randall-Sundrum gravitons (G), a heavy W boson (W'), and a heavy Z boson (Z').

Excited quarks (q^*) are spin 1/2 particles that are strongly produced giving large cross sections ($qg \rightarrow q^*$). The parton level angular distribution is $dN/d\cos\theta^* \sim 1+\cos\theta^*$, where θ^* is the angle between the initial and final state quark in the center of momentum frame. However, in proton-proton collisions the incoming quark comes equally from either proton and hence from either direction in z, yielding equal amounts of negative and positive values of $\cos\theta^*$ for any observed final state quark. So the $\cos\theta^*$ term cancels yielding an isotopic angular distribution $dN/d\cos\theta^* \sim 1$ for excited quark decays to dijets. We note that E_6 diquarks will also have isotropic angular distributions, since they are scalar particles.

There are many spin 1 particles that couple to $q\bar{q}$. Axigluons (A) or colorons (C) are strongly produced with large cross sections ($q\bar{q} \rightarrow A$ or C). Heavy gauge bosons, Z' and W', are electroweakly produced yielding small cross sections ($q\bar{q} \rightarrow Z', q_1\bar{q}_2 \rightarrow W'$). The dijet angular distribution for all these vector particles decaying to fermions is $dN/d\cos\theta^* \sim 1 + \cos^2\theta^*$.

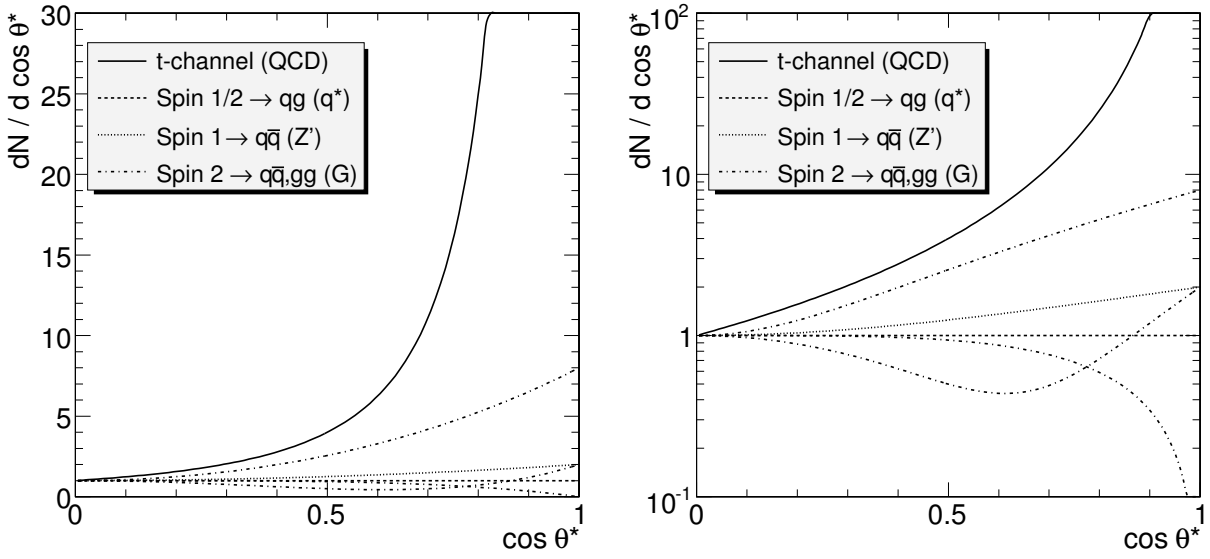

Figure 2: Left) Angular distributions for a t-channel term are compared to those from dijet resonances of Spin 1/2, 1 and 2. Right) Same with a logarithmic vertical axis.

Randall-Sundrum gravitons (G) are spin 2 particles produced from gluons or quark-antiquark pairs in the initial state ($q\bar{q}, gg \rightarrow G$). Their cross sections are small and their angular distributions depend on the sub-process considered [5]

- for $q\bar{q} \to G \to q\bar{q}$, $dN/d\cos\theta^* \sim 1 - 3\cos^2\theta^* + 4\cos^4\theta^*$
- for $gg \to G \to gg$, $dN/d\cos\theta^* \sim 1 + 6\cos^2\theta^* + \cos^4\theta^*$
- for $gg \to G \to q\bar{q}$ or $q\bar{q} \to G \to gg$, $dN/d\cos\theta^* \sim 1 - \cos^4\theta^*$

In Figure 2 these resonance angular distributions are compared to the t-channel term which dominates the QCD background, $dN/d\cos\theta^* \sim 1/(1-\cos\theta^*)^2$. Compared to the irreducible QCD background all these angular distributions are relatively isotropic: pretty flat in $\cos\theta^*$.

1.2.2 Contact Interactions

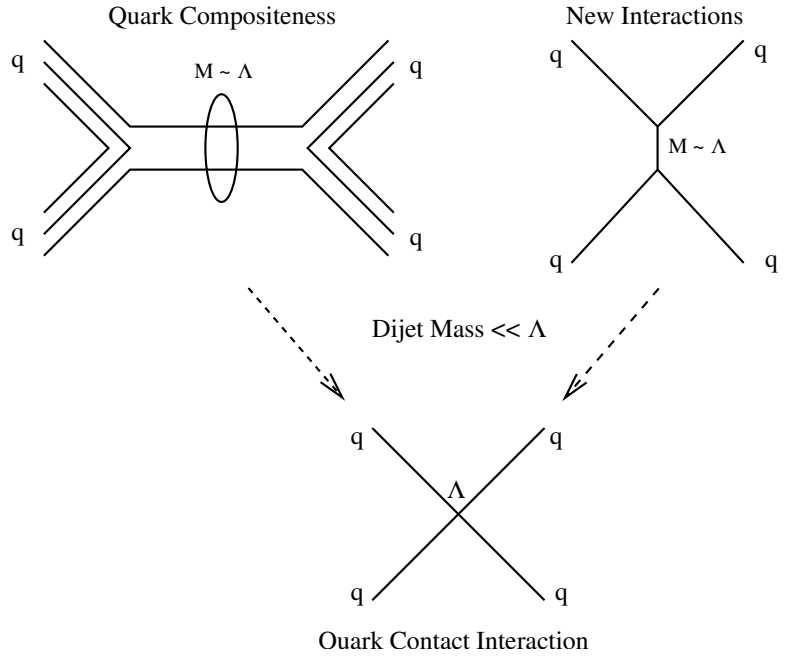

Figure 3: Schematic picture of the origin of quark contact interactions from either quark compositeness or any model of new interactions among quarks.

New physics at a scale Λ above the mass of the final state is effectively modeled as a contact interaction, as pictured in Figure 3. Contact interactions produce a rise in rate relative to QCD at high dijet mass or high inclusive jet p_T as shown in Figure 3. They can also produce observable effects in the dijet angular distributions, which benefit from much smaller measurement systematic uncertainties. The canonical contact interaction studied in hadron collisions arises from the following left-left isoscalar color-singlet term which is added to the QCD Lagrangian [6]:

$$L_{qq} = \frac{Ag^2}{2\Lambda^2}(\overline{q}_L\gamma^\mu q_L)(\overline{q}_L\gamma_\mu q_L) \quad (1)$$

where $A = \pm 1$ will determine the sign of the interference with QCD, Λ is the contact interaction scale, and the square of the coupling g^2 is by convention set equal to $4\pi\alpha_s$. $\Lambda^\pm$ is compact notation commonly used for Λ with the choice $A = \pm 1$.

1.3 Monte Carlo Samples and Theoretical Calculations

This analysis uses a QCD sample of one million events without pileup produced with software from CMSSW_1_2_0. The events were generated with PYTHIA 6.227 using the Tune DWT for underlying event parameters [10]. The sample was generated in 21 bins of the transverse momentum in the parton hard-scatter, $\hat{p}_T$, which span the full kinematic range. Each $\hat{p}_T$ sub-sample has a weight corresponding to the generated cross section per event for that sub-sample. When making histograms all events from each sub-sample are used along with their corresponding weight and all errors are calculated taking into account the weights, as described previously [2]. Some of the figures, if noted in the caption, use the Spring07 QCD sample that was generated and simulated with CMSSW_1_2_3

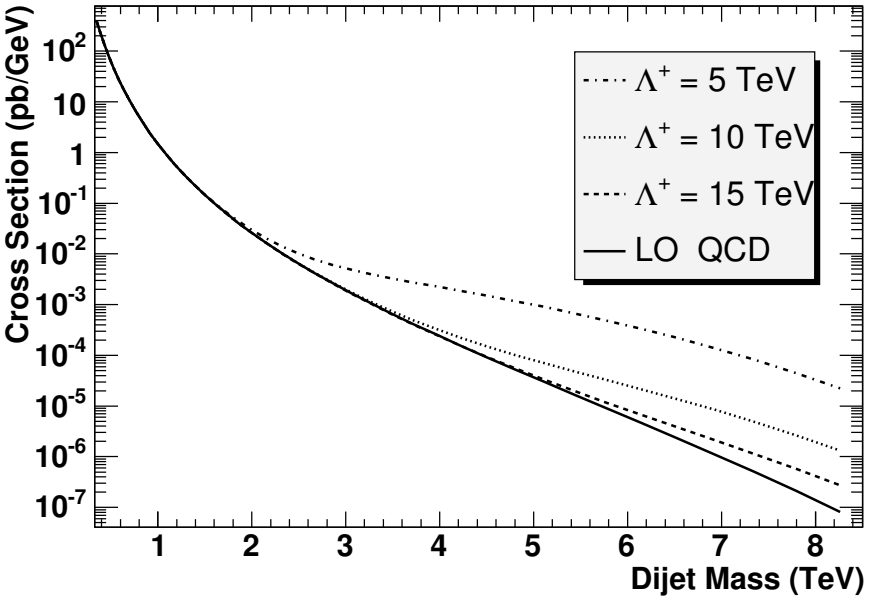

Figure 4: A lowest order calculation of the dijet mass distribution for $|\eta| < 1$ from QCD (solid) and from QCD plus a contact interaction with scale Λ of 5 TeV (dot-dash), 10 TeV (dotted), and 15 TeV (dashed) and destructive interference term ($A = +1$).

and digitized and reconstructed with CMSSW_1_3_1. Other figures, if noted in the caption or text, use a lowest order QCD calculation. Otherwise, all QCD results use the CMSSW_1_2_0 sample.

This analysis uses three different types of samples for dijet resonances. A CMSSW_1_2_0 resonance sample was produced by the LPC MC production group at the Fermilab Tier1. It was a full CMS simulation of Z' decaying to dijets for three different resonance masses: 4000 events at $M = 0.7$ TeV, 3000 events at $M = 2$ TeV, and 3000 events at $M = 5$ TeV. It is used for the analysis in sections 4.1, 4.2, 4.3. A Spring07 resonance sample was generated and simulated with CMSSW_1_2_3 and digitized and reconstructed with CMSSW_1_3_1. It was also a full CMS simulation of Z', at $M = 0.7$, 2 and 5 TeV but with better statistics: 30 thousand events for each mass. It is used for the analysis in section 4.4 and for Corrected CaloJets in section 5.4. To study angular distribution dependence a private sample was generated and reconstructed with CMSSW_1_4_0 for three different resonance types (Z', q^*, and Randall-Sundrum gravitons) at the same three standard masses (0.7, 2 and 5 TeV). Each subsample contained 100 thousand events. This private sample was used for GenJet level analysis in section 5.4.

We generated samples of QCD plus a contact interaction using PYTHIA in CMSSW_1_2_0 with the same settings as for the QCD samples described above, except for including the contact interaction term. Samples were created for contact interaction scales Λ^+ =3,5,10 and 15 TeV. We chose the variant of the model where all three families of quarks are assumed to be composite and used $A = +1$ parameter, corresponding to destructive interference. Since we will see that the analysis of the QCD samples indicated good agreement between results from generated and corrected calorimeter levels, we did not employ the full detector simulation for the contact interaction samples, and used the generated-level distributions instead. All the results on contact interactions using the dijet ratio employ this generator level sample. Some figures on inclusive jet p_T, if noted in the caption, use a lowest order calculation for contact interaction effects. Otherwise, all contact interaction results use the CMSSW_1_2_0 generated-level samples.

2 Jet Measurement

2.1 Jet Reconstruction and Energy Correction

Jets are reconstructed in data at the calorimeter level (CaloJets) and in Monte Carlo truth at the particle level (GenJets) using a cone algorithm. CaloJets are reconstructed from CaloTowers: energy deposits in the CMS calorimeters arranged in a projective tower geometry. The jet energy E is defined as the scalar sum of the calorimeter tower energies inside a cone of radius $R = \sqrt{(\Delta\eta)^2 + (\Delta\phi)^2} = 0.5$, centered on the jet direction. The iterative cone algorithm and the midpoint cone algorithm currently employed at CMS yield indistinguishable results for the dijet analysis we will consider. The jet momentum $\vec{p}$ is the vector sum of tower momenta in the jet, where the tower momentum vector points from the origin to the center of the tower and has a magnitude equal to the tower energy. The jet transverse energy is $E_T = E \sin\theta$, and the jet transverse momentum is $p_T = p \sin\theta$, where θ is the angle between the jet momentum and the proton beam. GenJets are similarly defined using the energy and momentum of the particles. Jet energy corrections [11] have been applied to CaloJets to obtain corrected CaloJets (CorJets) which have the same Lorentz vector as the corresponding GenJet on average. The multiplicative correction decreased with CaloJet E_T from 1.5 at $E_T = 70$ GeV to 1.1 at $E_T = 3$ TeV for CaloJets in the barrel region.

We define the dijet system as the two jets with the highest p_T in an event (leading jets) and define the dijet mass $m = \sqrt{(E_1 + E_2)^2 - (\vec{p_1} + \vec{p_2})^2}$. Unless otherwise noted, plots in this note that are a function of dijet mass use the same mass bins as in PTDR2 [4].

2.1.1 Optimal η Region

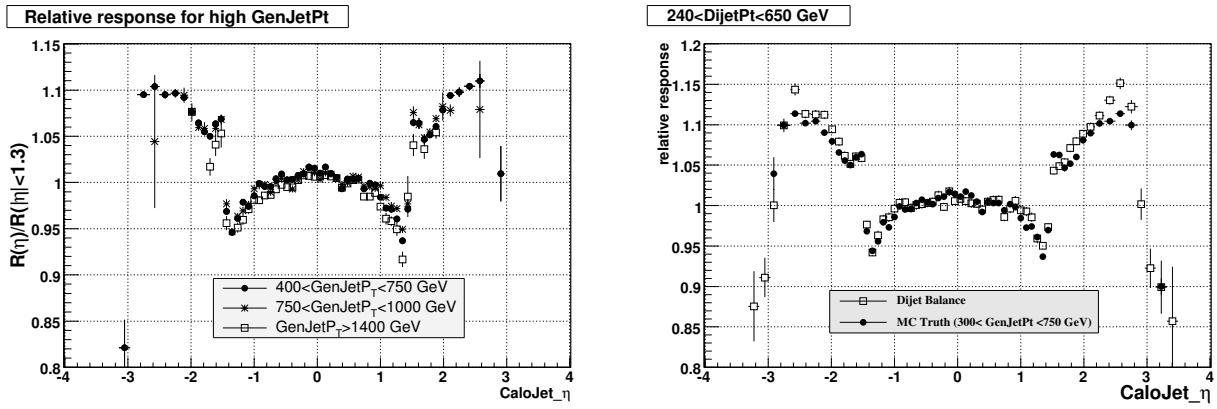

Figure 5: Left) The jet response relative to the region $|\eta| < 1.3$ as a function of CaloJet η shown for three different bins of GenJet p_T. Right) The relative jet response determined from dijet balance is compared to the relative jet response from MC truth for the appropriate GenJet p_T. Both plots are from the Spring07 QCD simulation sample.

Our searches will only use jets where the jet axis is inside the CMS barrel calorimeter. Specifically, analysis has been done with two cuts, $|\eta| < 1$ which was inherited from Tevatron analysis and used in the physics TDR [1], and $|\eta| < 1.3$ which is our new optimized cut for CMS. One reason why an $|\eta|$ cut is applied is that new physics is produced at small $|\eta|$. Section 4.3 shows that a cut of $|\eta| < 1.3$ optimizes our statistical sensitivity to dijet resonances in the dijet mass distribution. Another important reason is that the response of the detector is not uniform as a function of η, and including jets outside the CMS barrel will increase our systematic uncertainties. Figure 5 illustrates that the relative jet response in the simulation varies smoothly within the barrel, decreasing by about 5% as the jet $|\eta|$ increases from 0 to $|\eta| < 1.3$. As the jet enters the transition region between the barrel and the endcap, the jet response changes rapidly, increasing by around 10% in the interval $1.35 < |\eta| < 1.5$. We anticipate that the source of this variation in simulation response will also be a source of systematic uncertainty in our measurement. To illustrate the complexity of the calorimeter for the region just outside $|\eta| = 1.3$, we note the following

- CaloTowers 1-15 which span $|\eta| < 1.305$ are made only from the barrel Ecal, barrel Hcal and the HO, so uniform response is expected.
- CaloTower number 16 which spans $1.305 < |\eta| < 1.392$ is a complex interleaving of both the Hcal barrel

(two depths) and the Hcal endcap (one depth in back) and is the first tower that does not have the HO.

- CaloTower number 17 which spans $1.392 < |\eta| < 1.479$ is the first tower in the Hcal endcap, and uses the Ecal barrel.
- CaloTower number 18 which begins at $|\eta| = 1.479$ is the first tower in the Ecal endcap.

We believe that understanding the response in this transition region will be challenging and will not be achieved in the first days of CMS running. We recommend that the first jet analysis at CMS searching for new physics be within the region $|\eta| < 1.3$ to minimize systematic uncertainty. We show in section 4.3 that this also optimizes our statistical sensitivity for dijet resonances in a search using the total rate within an $|\eta|$ cut.

The way we plan to understand the jet response vs. η is to use dijet p_T balance in the actual collision data [12]. Figure 5 shows that dijet p_T balance, with one jet in the control region $|\eta| < 1.3$, gives the same measured relative detector response as expected from MC truth. Measurements of dijet balance using actual collision data will enable us to test whether the detector simulation of jet response versus η are reliable. The first dijet balance data will tell us what is the η region of smoothly changing calorimeter response and we can adjust our cuts if necessary.

2.2 Trigger and Datasets

2.2.1 Triggers used for Analysis

In the physics TDR we proposed a single jet trigger table [7]. It was designed following these principles

1. We need multiple trigger thresholds and prescales to measure a full spectrum with limited bandwidth.
2. The thresholds need to be spaced to provide reasonable overlap for high statistics measurement of trigger efficiency and cross check of prescale values.
3. The sizes of the samples need to be balanced to provide good measurement statistics without creating datasets so large that they cannot be easily analyzed.
4. We need to provide for the evolution of the trigger by adding thresholds, never moving them, and increasing prescales as necessary.

Path	L1				HLT		ANA
	E_T Cut (GeV)	Unpres. Rate (KHz)	Prescale (N)	Presc. Rate (KHz)	E_T Cut GeV)	Rate (Hz)	Dijet Mass (TeV)
Triggers for 10^{32}cm^{-2}s^{-1} and integrated luminosity = 100 pb^{-1}							
High	140	0.044	1	0.044	250	2.8	>0.67
Med	60	3.9	40	0.097	120	2.4	0.33-0.67
Low	25	2.9 $\times 10^2$	2,000	0.146	60	2.8	None
Triggers for 10^{33}cm^{-2}s^{-1} and integrated luminosity = 1 fb^{-1}							
Ultra	270	0.019	1	0.019	400	2.6	>1.13
High	140	0.44	10	0.044	250	2.8	0.67-1.13
Med	60	39	400	0.097	120	2.4	0.33-0.67
Low	25	2.9 $\times 10^3$	20,000	0.146	60	2.8	None
Triggers for 10^{34}cm^{-2}s^{-1} and integrated luminosity = 10 fb^{-1}							
Super	450	0.014	1	0.014	600	2.8	>1.80
Ultra	270	0.19	10	0.019	400	2.6	1.13-1.80
High	140	4.4	100	0.044	250	2.8	0.67-1.13
Med	60	3.9 $\times 10^2$	4,000	0.097	120	2.4	0.33-0.67
Low	25	2.9 $\times 10^4$	200,000	0.146	60	2.8	None

Table 2: The Physics TDR single jet trigger table [7],showing path names, trigger thresholds in corrected E_T, prescales, estimated rates at L1 and HLT for three different luminosity scenarios, and here we also list the corresponding range of corrected dijet mass used in this analysis.

Path	L1				HLT	
	p_T Cut (GeV)	Unpres. Rate (KHz)	Prescale ($\div N$)	Presc. Rate (Hz)	p_T Cut (GeV)	Rate (Hz)
Single-Jet Pre#1	30	60	10,000	6	60	0.8
Single-Jet Pre#2	70	2.8	100	28	110	1.5
Single-Jet Pre#3	100	0.5	1 (HLT = 10)	500	150	3.6
Single-Jet Unprescaled	150	0.065	1	65	200	9.6

Table 3: The single jet trigger table from the spring 2007 HLT exercise.

Path	L1				HLT	
	p_T Cut (GeV)	Unpres. Rate (KHz)	Prescale ($\div N$)	Presc. Rate (Hz)	p_T Cut (GeV)	Estimated Rate (Hz)
Single-Jet Pre#1	30	60	500	120	60	5.4
Single-Jet Pre#2	70	2.8	40	70	110	4.0
Single-Jet Pre#3	100	0.5	5	100	180	3.3
Single-Jet Unprescaled	150	0.065	1	65	250	3.3

Table 4: An example of a jet trigger table with the different streams balanced more like one would prefer for normal data taking

In table 2 we list the trigger table from the physics TDR dijet mass analysis [4] and the dijet mass range that we will analyze from each trigger for the cut $|\eta| < 1$. Unless otherwise noted, the sensitivity estimates in this analysis use the triggers with the prescales listed here to define their statistical uncertainties for a given sample size. Sensitivity estimates for instantaneous luminosities of $10^{31}\text{cm}^{-2}\text{s}^{-1}$ and integrated luminosities of 10 pb^{-1}, not considered when this trigger table was designed, used this table for $10^{32}\text{cm}^{-2}\text{s}^{-1}$ but with the prescales of the Med trigger reduced to 4 from 40 and the prescales of the Low trigger reduced to 200 from 2000.

2.2.2 Triggers in use for CMS exercises

The CMS analysis exercises in 2007, both the HLT exercise and CSA07, use the trigger table shown in table 3. This trigger table served well the goals of those exercises. We feel the table could be improved for analysis by modifying the HLT thresholds and prescales to better balances the output rates with slightly more emphasis on low p_T rates for dijet balance and studies of lower p_T jets which produce fake leptons or photons. The better balanced rates will also lead to larger overlap among the triggers, needed both for measuring trigger efficiencies and for checking prescales with the data. As described in the jet trigger study for the physics TDR [7], with each trigger we will measure the efficiency of the trigger at the next higher p_T, and the events at the tail of the lower p_T trigger which overlap with the higher p_T trigger go into the denominator of the trigger efficiency and therefore determine the statistical precision of the efficiency we can measure. We also feel that a rate of 10 Hz for the highest p_T jet trigger is a little excessive because it makes this critical data sample for new physics searches difficult to analyze quickly. We recommend reducing the rate by moving the threshold up slightly. In table 4 we propose a trigger table that is one example of a way to implement these improvements. Note that it balances the rates with a slightly larger rate at lower p_T where additional events are needed for dijet balance, fake rate studies, and to insure overlap for trigger efficiency.

2.2.3 Primary Datasets

It is important that each of the single jet trigger paths correspond to a single unique primary dataset, inclusive of all events that satisfy that trigger. For example, if the physics TDR trigger for $10^{32}\text{cm}^{-2}\text{s}^{-1}$ were used, there would be three primary datasets: the LowEtJet, the MedEtJet and the HighEtJet. Every event in the LowEtJet dataset would have passed the LowEtJet trigger, and similarly for the MedEtJet and HighEtJet samples. Overlaps between the samples are small as a fraction of total rate, but very important that they be kept in order to measure the trigger efficiency and check the prescales. We do not recommend trying to save a little storage space by producing exclusive datasets which do not duplicate event storage, because this is a false economy which will end up taxing rather than saving computing resources, because users will be forced to access multiple exclusive datasets to get all the events that satisfy a single trigger. The reasons why we recommend that each jet trigger path have its own dataset are the following:

1. All single jet triggers individually produce a large quantity of data. If they were all combined in a single dataset it would be very difficult to access and analyze all this data.

2. The first step in using the data for analysis is having a dataset in which every event passed a particular single jet trigger. Then we have a well defined trigger sample from which we can measure trigger efficiencies and check prescales. Further, then we know this sample needs to be corrected for a specific prescale and trigger efficiency. It is useful if this first step defines a dataset that the entire collaboration can access, since everybody will have to face this issue.

3. The individual triggers are often used for different purposes, for which it is useful to have them divided in advance. Low p_T triggers are needed by the entire collaboration for studies of the rate of a jet faking a lepton or photon and for dijet balance to determine the response of the forward region. High p_T jet triggers are pretty much only of interest to QCD jet measurements and high p_T searches, so they could be separated out from the triggers of more general use. For these analyses you want a manageable size dataset for the high p_T end of the spectrum.

One of the largest challenges of jet analysis in the beginning of the run is just processing and accessing all the data. This task can be made much easier by splitting the data according to jet trigger path into inclusive datasets before analysis begins.

2.3 Jet Cleanup

In addition to jets that originate from the hard scattering of partons, we will likely observe large calorimeter signals originating from occasional occurrences of catastrophic noise, beam-halo energy deposits, and cosmic ray air showers. While their rate of occurrence may be small compared to low p_T jets, it could be significant compared to higher p_T jets. One thing all these noise sources share in common is that unlike dijets they most often produce large amounts of missing E_T (MET) compared to the total E_T (ΣE_T) in the event. In Figure 6 we show the distribution of MET/ΣE_T for a $\hat{p_T}$ bin of the QCD sample. The distribution is peaked at low MET/ΣE_T, characteristic of a dijet event. Figure 6 demonstrates that a cut requiring MET/$\Sigma E_T < 0.3$ is safely more than 99% efficient for QCD dijets at all values of $\hat{p_T} > 20GeV$. When we start taking data, we recommend a cut such as this to reject very high E_T jets from catastrophic noise, beam-halo, or cosmic rays without biasing the shape of our QCD spectrum. The inclusive jet p_T analysis that follows applies this cut for fully simulated events.

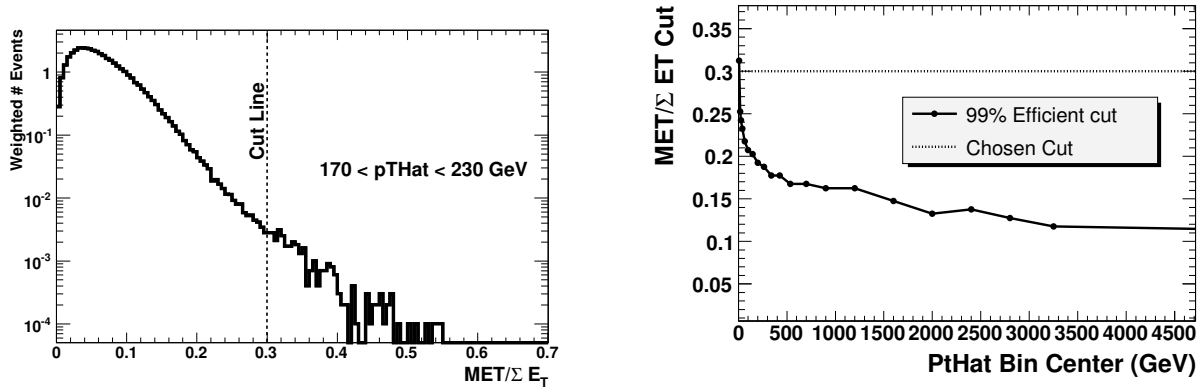

Figure 6: Left) The distribution of MET/ΣE_T is shown for a QCD dijet sample with $170 < \hat{p_T} < 230$ GeV along with the position of a cut requiring MET/$\Sigma E_T < 0.3$. Right) The value of a cut on MET/ΣE_T that is 99% efficient for QCD dijets is plotted as a function of the hard scatter transverse momentum $\hat{p_T}$ and compared to a flat cut at MET/$\Sigma E_T < 0.3$

3 Inclusive Jet p_T

3.1 QCD background

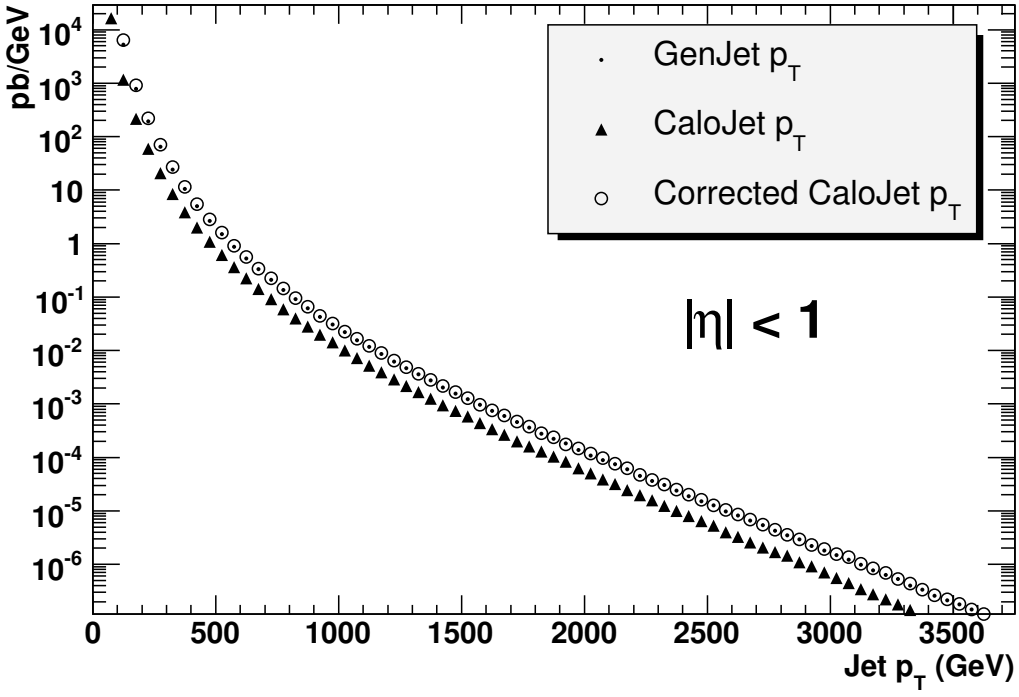

Figure 7: The inclusive jet differential cross section as a function of jet p_T is shown for GenJets, CaloJets and Corrected CaloJets for jet $|\eta| < 1$.

The inclusive jet cross section is a simple measurement of the probability for finding a jet as a function of jet p_T in an η region of the detector. We concentrate on the barrel, where we have results for $|\eta| < 1$ now, and we plan to study the region $|\eta| < 1.3$ in the future. In Figure 7 we show the cross section falls steeply with increasing p_T, dropping by 12 orders of magnitude in the interval $100 < p_T < 3500$ GeV. The cross section for CaloJets is less than the cross section for GenJets, because the CaloJet p_T is less before jet energy corrections. Figure 7 shows that after jet energy corrections are applied, the cross section for corrected CaloJets is very close to the cross section for GenJets. In Figure 8 we show the ratio between the cross section for corrected CaloJets and for Gen Jets. Since the goal of the jet energy correction was the GenJet energy, the rates agree fairly well, and the ratio is about 1. Even for a perfect correction we would expect some difference due to the resolution smearing on a falling spectrum: the migration of jets from a lower p_T bin to a higher p_T bin due to upward fluctuations in energy from lower p_T values where jets are plentiful to higher p_T values where jets are scarce. While it is unclear how much of an effect to attribute to energy corrections, and how much to attribute to resolution smearing, we adopt a pragmatic approach where whatever is left over after jet energy corrections is attributed to resolution smearing. Figure 8 is then defined as the resolution smearing affect on the jet cross section, and dividing the measured cross section by this gives a cross section that is corrected for resolution smearing. We note that this is a rather simplified approach to deconvolution, but it is straightforward and should suffice for a first measurement and correction of the inclusive jet p_T spectrum. We are encouraged by the fact that for this version of the jet energy corrections the resolution smearing appears to be a small effect, and we expect its systematic uncertainties will therefore also be small.

3.2 Uncertainties

The largest uncertainty in the inclusive jet cross section arises from the uncertainty in the jet energy scale. Systematic uncertainties in the jet energy scale are effectively multiplied by the slope of the cross section as a function of p_T to obtain the uncertainty on the cross section. In Figure 9 we show a lowest order QCD calculation of the shift in the cross section arising from of a shift in the jet p_T of 1%, 5% and 10%. For example, for a 5% upward shift in jet p_T the observed cross section increases between 30% at $p_T = 150$ GeV to 80% at jet p_T of 3 TeV. Also in

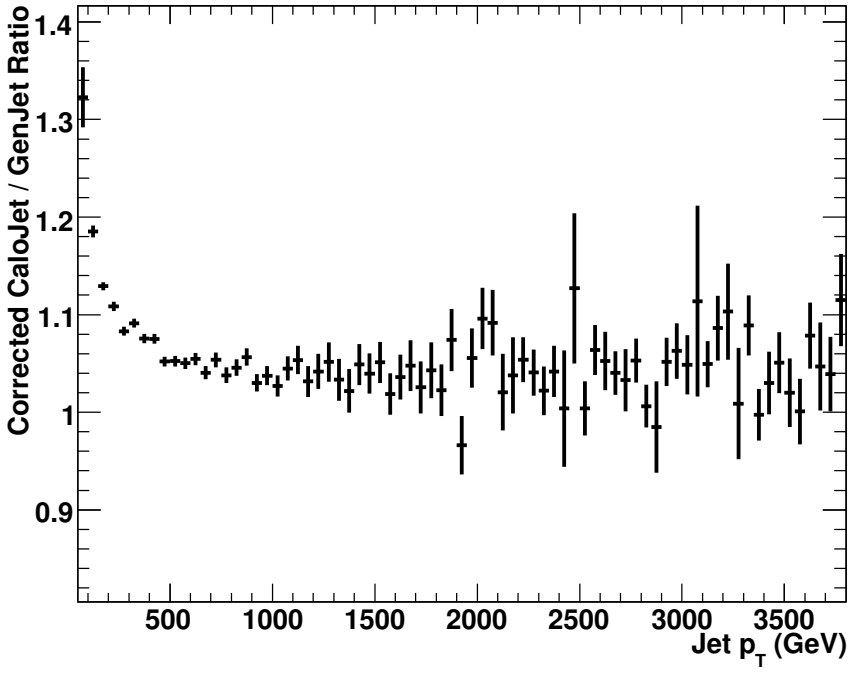

Figure 8: The ratio between the cross section for Corrected CaloJets and for Gen Jets as a function of jet p_T.

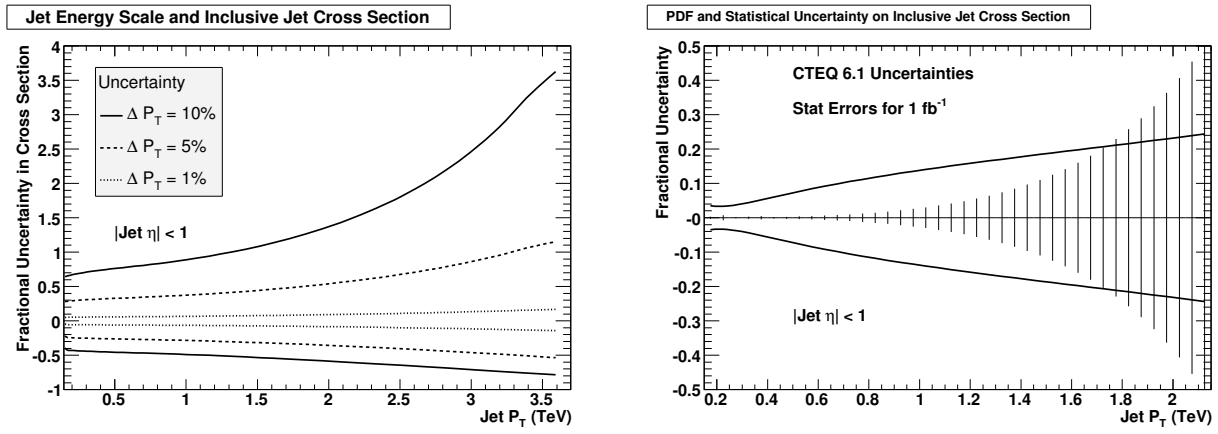

Figure 9: Left) Lowest order calculation of the fractional uncertainty in the inclusive jet cross section arising from a percent uncertainty in jet P_T of 10% (Solid), 5% (dashed) or 1% (dotted) is shown as a function of jet p_T. Right) The uncertainty in the expected inclusive jet cross section arising from PDF systematic uncertainties evaluated by the CTEQ collaboration for set 6.1 (solid) is compared with the statistical uncertainties for 1 fb^{-1}.

Fig. 9 we show the expected uncertainty in the lowest order QCD calculation due to parton distributions systematic uncertainties, and compare that with the expected statistical uncertainties from a 1 fb^{-1} sample using the physics TDR trigger. While the PDF uncertainties are in the QCD prediction and not in our measurement, they still affect our ability to compare our measurement with the QCD prediction, and hence to find our exclude any new physics that might be present. While Figure 9 shows that we will have clear statistical sensitivity to PDF variations with 1 fb^{-1} of data, it will require energy scale errors of roughly 2% or less for CMS to be sensitive to PDF variations at the level expected by the systematic uncertainties predicted by CTEQ 6.1. These systematics are consistent with those previously reported in a physics TDR study [7] for uncertainties as a function of dijet mass.

3.3 Sensitivity to Contact Interactions

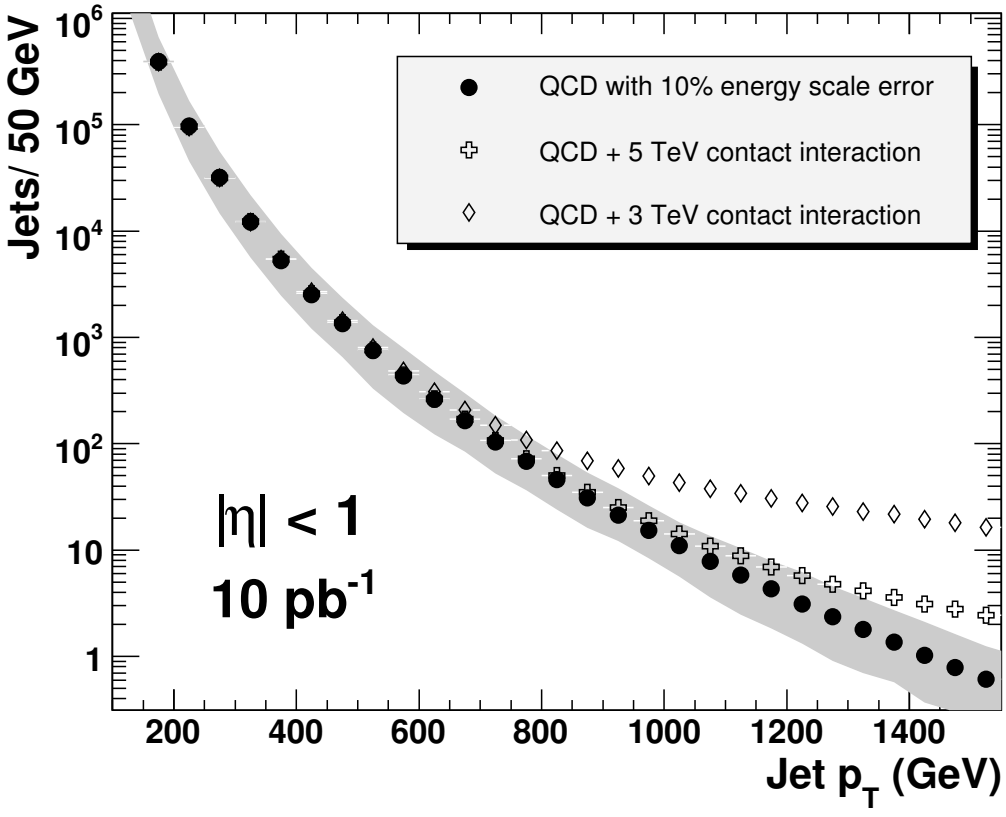

Figure 10: The inclusive rate for GenJets in 50 GeV bins for an integrated luminosity of 10 pb^{-1} is compared for QCD and for a contact interaction with various values of the scale Λ^+. The effect of a 10% energy scale error is shown as a shaded band.

We have looked at our sensitivity to contact interactions using both a GenJet level simulation and using a lowest order QCD calculation. Figure 10 shows the jet rates at GenJet level expected for an integrated luminosity of 10 pb^{-1}. A contact interaction with scale $\Lambda^+ = 3$ TeV clearly produces a large rate compared to QCD for jet $p_T > 1$ TeV, even taking into account a 10% energy scale uncertainty. Figure 11 shows a lowest order calculation of the effect of a quark contact interaction on the inclusive jet cross section compared to estimates of the uncertainties. We can see that very early in the run, when we anticipate quickly accumulating an integrated luminosity of 10 pb^{-1}, a $\Lambda^+ = 3$ TeV contact interaction will produce a remarkable signal for jets with p_T of around 1 TeV or greater. This signal will be clearly visible above the cross section systematic uncertainty caused by an estimated 10% systematic uncertainty in the jet energy scale at turn on of the experiment. The Tevatron has excluded $\Lambda^+ < 2.7$ TeV [13], so there is a clear possibility of discovery in the first data sample. After about a year of running, and 1 fb^{-1} of collision data, we could reasonably expect the systematic uncertainties on the jet energy scale to have been reduced to around 5% via various jet calibrations performed in-situ. Figure 11 shows that with this lower systematic uncertainty on the jet energy scale we will have some sensitivity to contact interaction scales around

$\Lambda^+ = 10$ TeV. Given the large systematic uncertainties present in the inclusive jet analysis it is difficult to quantify our sensitivity any further. Nevertheless, it appears quite clear that there are signals large enough to be convincingly seen in this distribution, and we certainly must measure it as a first simple test of both QCD and our understanding of the jet energy scale at CMS.

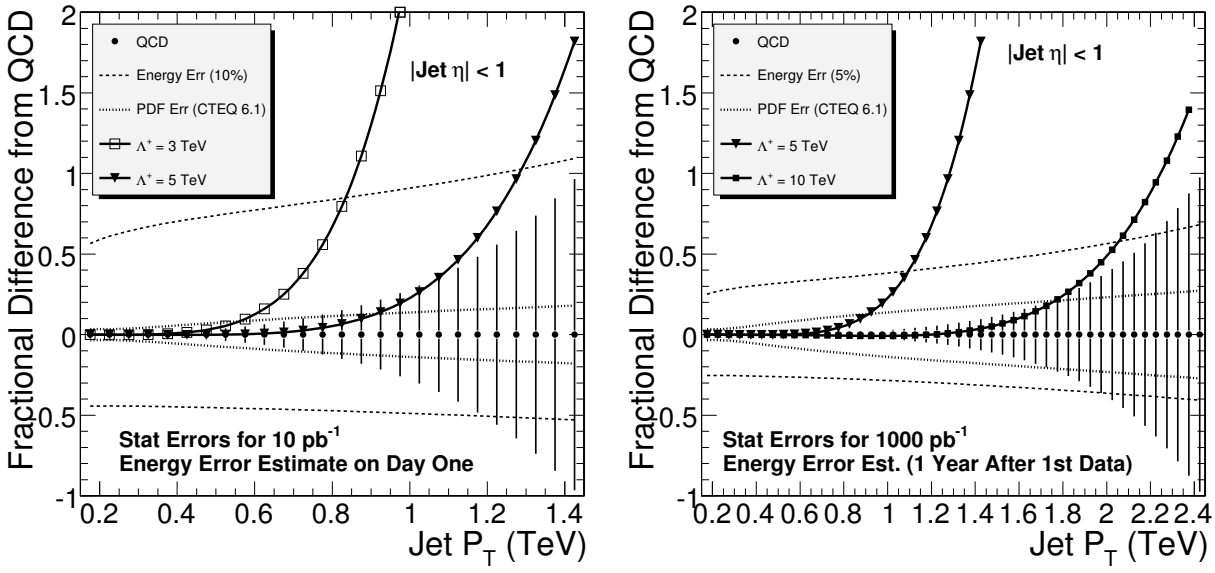

Figure 11: Left) Lowest order calculation of the fractional difference from QCD for the inclusive jet cross section arising from a 3 TeV and 5 TeV contact interaction is compared with the variation in QCD expected from PDFs, and from an energy scale error of 10%, and a statistical error on QCD corresponding to 10 pb^{-1}. Right) Same, but for a 5 TeV and 10 TeV contact interaction, and an energy scale error of 5%, and a statistical error corresponding to 1 fb^{-1}.

4 Dijet Mass

Measurements of rate versus dijet mass are the usual method of searching for dijet resonances. In sections 4.1- 4.3 we summarize 2007 analysis results presented in more detail elsewhere [2]. In section 4.4 we present a recent study of the dijet mass resolution. Systematic uncertainties were presented previously in studies for the physics TDR [4].

4.1 QCD Background

In Figure 12 we show the QCD differential cross section as a function of dijet mass for GenJets, CaloJets and corrected CaloJets. As for the inclusive jet cross section, the dijet mass cross section for CaloJets is much less than the cross section for GenJets and the cross section for corrected CaloJets is similar to the cross section for GenJets.

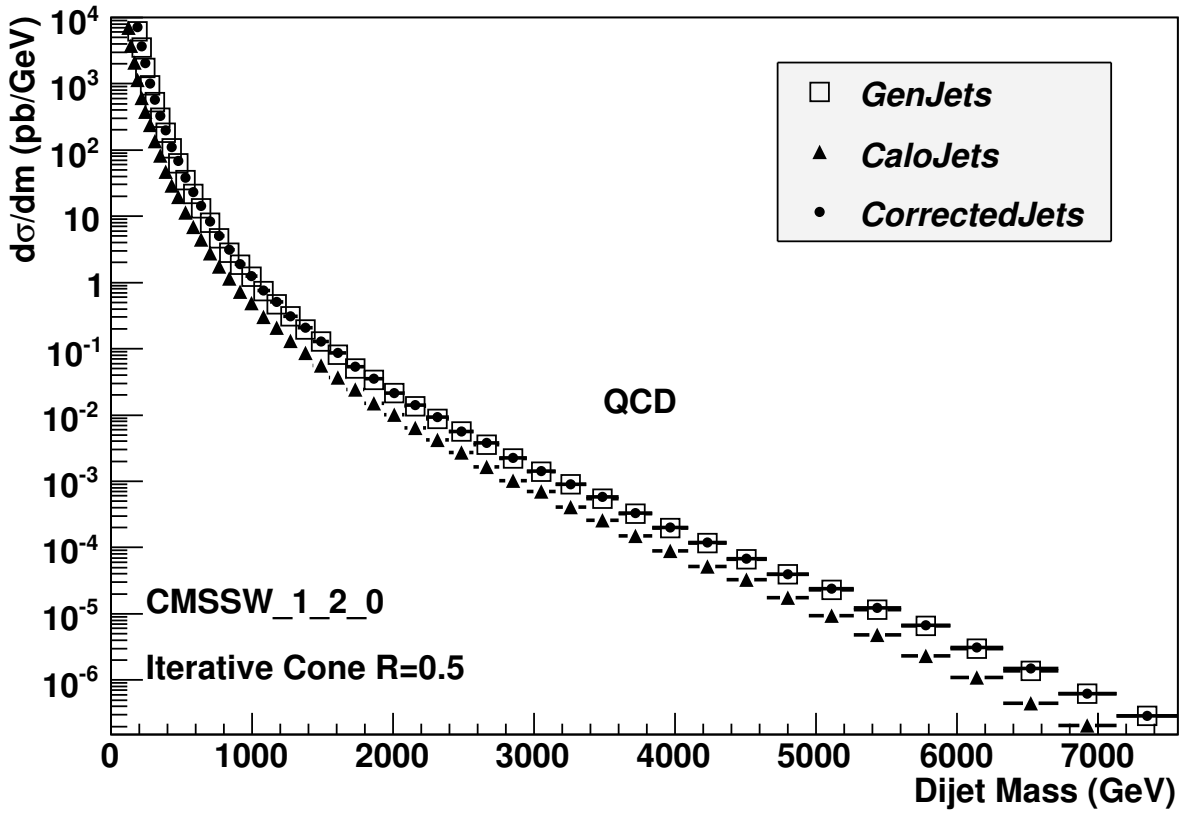

Figure 12: QCD differential cross section as a function of dijet invariant mass for $|\eta| < 1$ are shown for GenJets, CaloJets, and corrected CaloJets.

4.2 Sensitivity to Dijet Resonances

In Figure 13 we compare the cross section for an excited quark dijet resonance signal to the statistical uncertainties expected on the QCD dijet background for three luminosity scenarios: 10 pb^{-1}, 100 pb^{-1} and 1 fb^{-1}. The normalization of the excited quark signal came from our lowest order calculation [4] and the shape of the excited quark signal comes from a CMS simulation of dijet resonances for corrected CaloJets. The statistical uncertainties on the QCD background was obtained for the expected rates of corrected CaloJets, coming from the cross sections in Figure 12 multiplied by the luminosities and trigger prescales.

Figure 13 shows we will be sensitive to an excited quark signal up to many TeV. With only 10 pb^{-1} we can see a 2 TeV excited quark signal beginning to emerge above our statistical error bars with a total significance of 4.1σ, neglecting systematic uncertainties. With 100 pb^{-1} the same 2 TeV signal has a convincing significance of 13 σ.

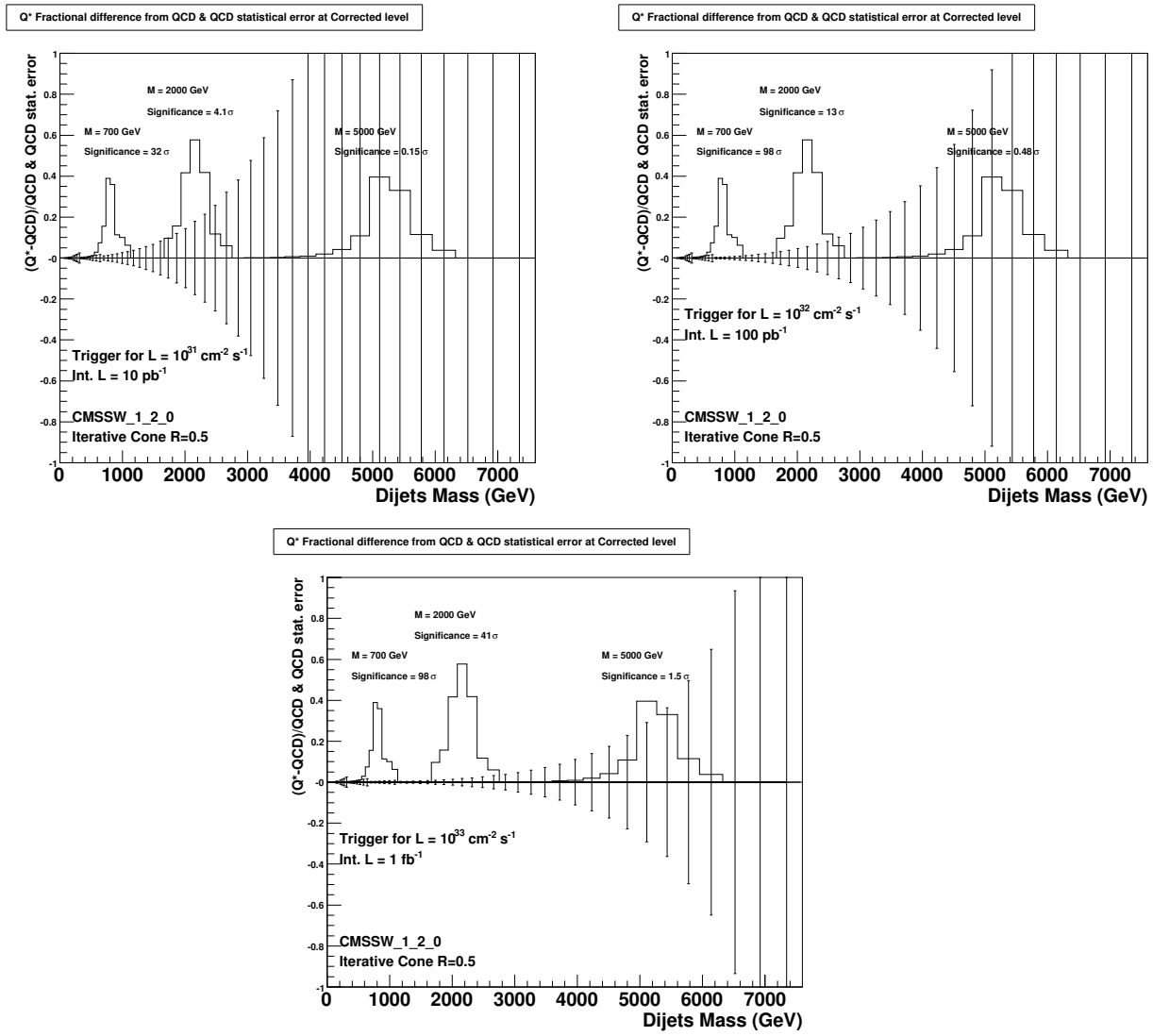

Figure 13: From dijet mass distributions with $|\eta| < 1$, the fractional difference between an excited quark signal and the QCD background compared to the QCD statistical error for an integrated luminosity of 10 pb^{-1} (top left plot), 100 pb^{-1} (top right plot) and 1 fb^{-1} (bottom plot).

In Figure 13 we list the total statistical significance for an excited quark signal at each resonance mass next to the mass peak on each plot. This total significance comes from summing the bin-by-bin significances in quadrature.

4.3 Optimization of η cut

The dijet resonance analysis presented so far required each leading jet to be in the region $|\eta| < 1.0$, just like in the physics TDR [1]. This cut was inherited from the Tevatron, but it was never optimized for CMS. Here we will estimate the optimal value of this cut for statistical sensitivity to dijet resonance signals. In Figure 14 we show the differential cross section as a function of dijet mass for the QCD background and a dijet resonance signal for 36 values of the $|\eta|$ cut, varying from $|\eta| < 0.5$ to $|\eta| < 4.0$ in steps of 0.1. As discussed previously [2], the signal considered has the total rate of an excited quark for the cut $|\eta| < 1$ and has the angular distribution from the decay of a spin 1 resonance. As we relax the eta cut from the default value of $|\eta| < 1.0$ to higher values, up to $|\eta| < 4.0$, the QCD background cross section increases by nearly three orders of magnitude. This is because QCD is dominated by t-channel scattering, simple Rutherford-like scattering, which peaks in the forward direction. In contrast the dijet resonance signal increases only slightly as we relax the $|\eta|$ cut from 1 to 4, because dijet resonance production is an s-channel process, which is always more isotropic and hence more centrally produced than a t-channel process. Hence we expect the sensitivity to be optimized by cutting at a relatively low value of η.

In Figure 14 we also show the total statistical significance of the signal compared to the background as a function of the $|\eta|$ cut for an integrated luminosity of 1 fb^{-1}. The significance is calculated by summing in quadrature the bin-by-bin statistical significance over all the bins of the resonance. The significance is calculated independently for each of three resonance masses, 0.7, 2, and 5 TeV. An $|\eta|$ cut of 1.3, shown by a vertical line in Figure 14, maximizes the significance for a 2 TeV resonance, and has a very similar significance as the maximum significance cut for a 0.7 and 5 TeV resonance as well. It is likely the best single value for an $|\eta|$ cut for this analysis, and we recommend its use in the future.

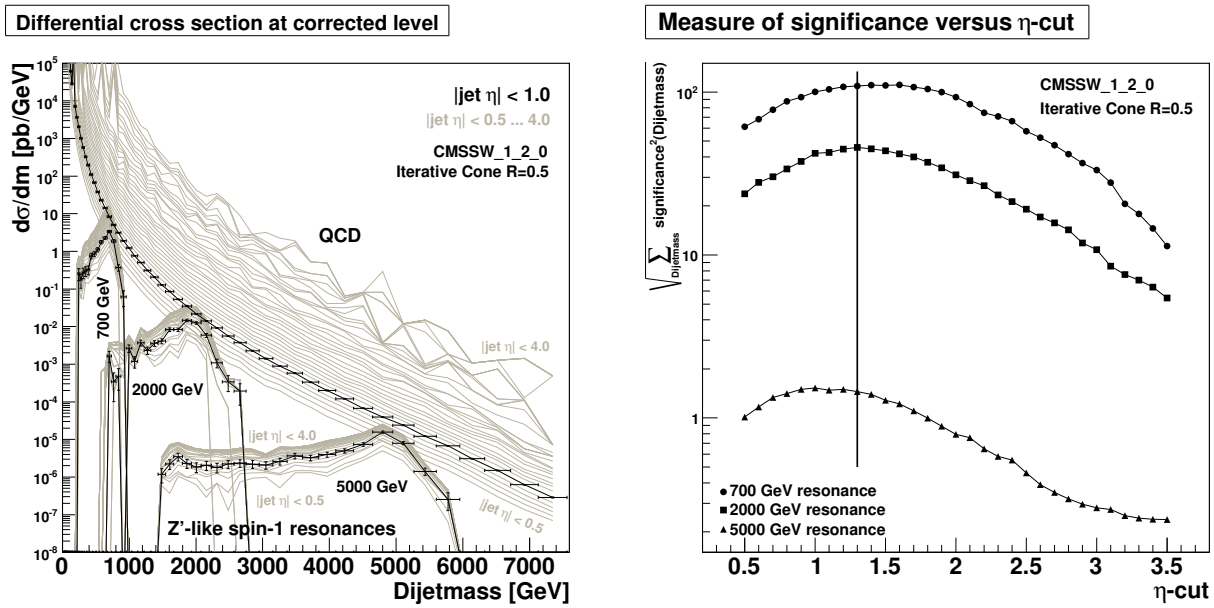

Figure 14: Left) The cross section for a dijet resonance signal and the QCD background as a function of dijet mass is shown for the cut $|\eta| < 1$ (points and dark curves) and for various values of the $|\eta|$ cut between 0.5 and 4.0 (light curves). Right) The statistical significance of a dijet resonance signal as a function of the $|\eta|$ cut for 1 fb^{-1} of integrated luminosity is shown for a resonance of mass 700 GeV (circles), 2000 GeV (squares) and 5000 GeV (triangles).

4.4 Dijet Mass Resolution with Optimized η Cut

The dijet mass resolution near the peak of a dijet resonance will significantly affect our sensitivity to the resonance in the presence of a large QCD background. Here we study the dijet mass resolution near the peak with a high statistics sample of Z' decaying to dijets and the cut $|\eta| < 1.3$. In Figure 15 we show the dijet mass distributions from a dijet resonance signal in fine bins of width 10 GeV. All distributions have a Gaussian core and a large tail at low mass caused by QCD radiation and PDF effects as discussed previously [4]. In Figure 15 we can explicitly see that the energy scale of CaloJets is lower than GenJets, and that jet corrections restore the original GenJet energy scale. We also see that the core of the distribution for GenJets, is narrower than that for Corrected CaloJets. These are fit with Gaussians in an asymmetric mass interval about the the mean, from -1σ to $+1.5\sigma$, and the fits are shown for corrected CaloJets. The resolution as a function of resonance mass, shown in Figure 16, varies from 9% at 700 GeV to 4.5% at 5000 GeV. The resolution can parameterized as a function of resonance mass, M in GeV,as

$$\frac{\sigma}{M} = 0.038 + \frac{38}{M} \tag{2}$$

within this mass region. Figure 16 shows that the resolution for the cut $|\eta| < 1$ and $|\eta| < 1.3$ is similar. This supersedes previous results shown in the physics TDR analysis [4] which quoted a poorer resolution at high resonance mass. Figure 16 also shows that the resolution for GenJets is significantly better than corrected CaloJets, and the natural width of the Z' resonance is even smaller. We recommend that future analysis searching for resonances at high dijet mass use bins that correspond to the expected resolution for corrected CaloJets presented here.

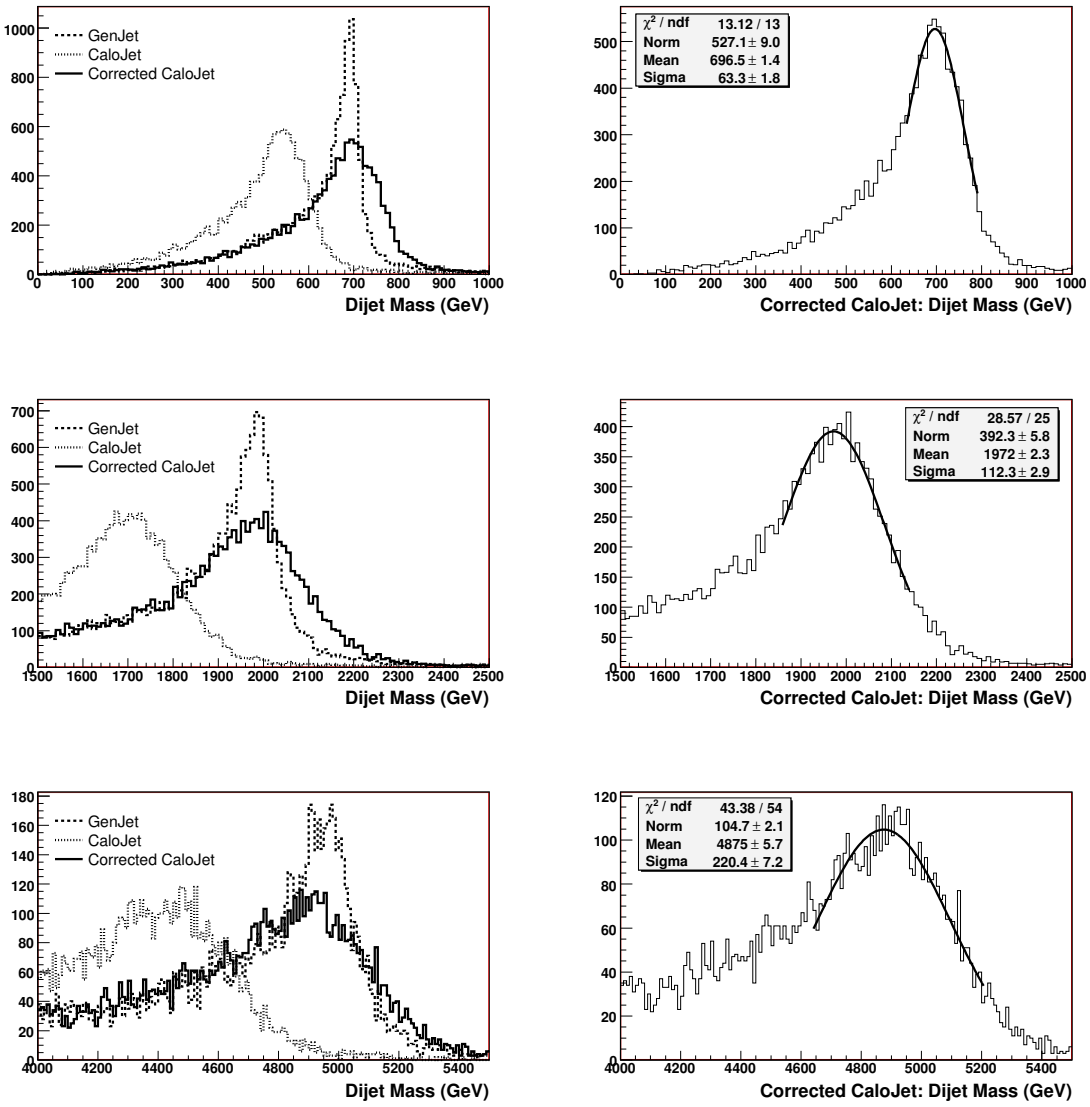

Figure 15: Dijet invariant mass for $|\eta| < 1.3$ from a Z' of mass 700 GeV (top), 2000 GeV (middle), and 5000 GeV (bottom). Plots on the left show histograms for GenJets (dots), CaloJets (thin dots), and corrected CaloJets (solid). Plots on the the right show the Corrected CaloJets fit with a Gaussian.

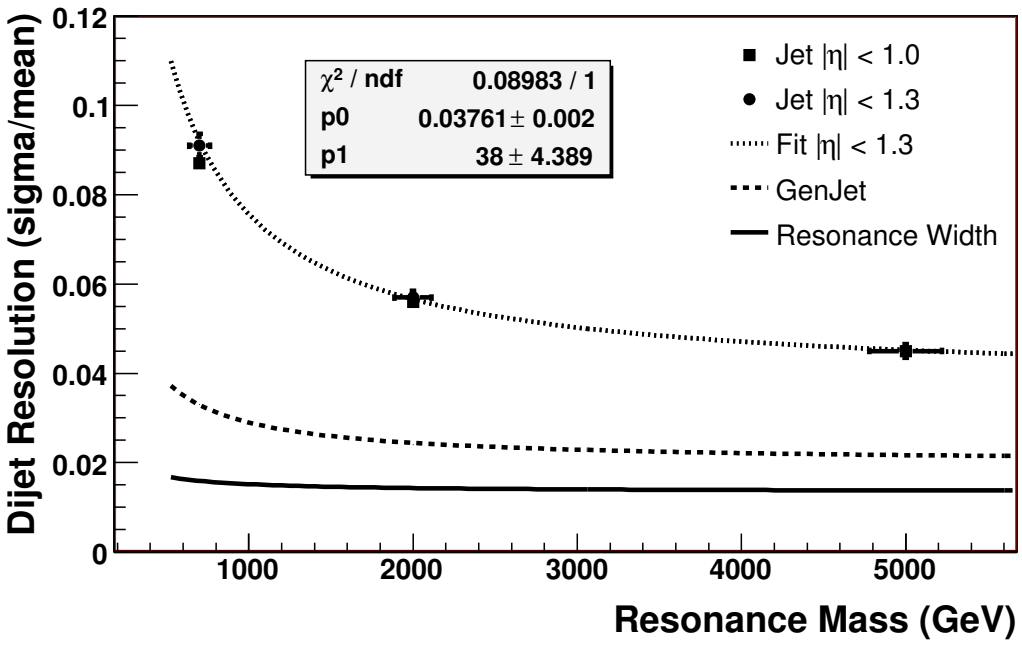

Figure 16: The dijet mass resolution for the resonance peak from Corrected CaloJets (points) are shown as a function of input Z' mass, M, and fit with a smooth parameterization (dotted) of the form $p_0 + p_1/M$. Also shown is the peak resolution for GenJets (dashed) and for the natural resonance line shape (solid).

5 Dijet Ratio

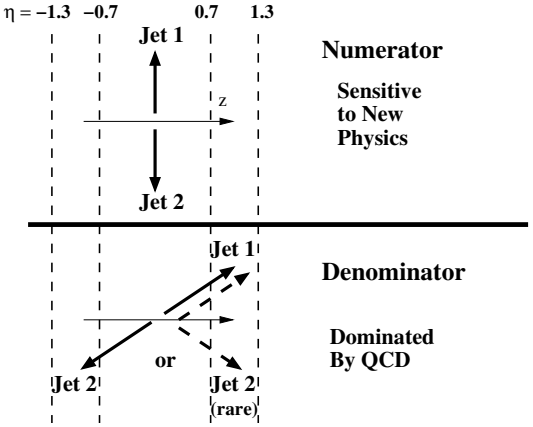

Figure 17: The η configuration of dijet events in the numerator and denominator of the dijet ratio.

Here we summarize the dijet ratio analysis [3]. The purpose of this analysis is to measure the dijet angular distribution as a function of dijet mass, to search for new physics emerging with mass (contact interactions) or appearing at a specific mass (resonances). The analysis uses the angular variable η, as opposed to $\cos\theta^*$, to keep the dijets within well defined regions of the calorimeter.

To characterize the shape of the angular distribution in a mass bin, we use the dijet ratio

$$N(|\eta| < \eta_{in})/N(\eta_{in} < |\eta| < \eta_{out}) \tag{3}$$

the ratio of the number of dijet events within an inner region $|\eta| < \eta_{in}$ to the number of dijet events within an outer region $\eta_{in} < |\eta| < \eta_{out}$. Both leading jets of the dijet event must satisfy the $|\eta|$ cuts. In this note we will show simulations of the dijet ratio for the values $\eta_{in} = 0.5$, $\eta_{out} = 1.0$, used in the original DØ analysis [13] and PTDR2 [1, 8], and for the values $\eta_{in} = 0.7$, $\eta_{out} = 1.3$, which we found to be optimal for a contact interaction search within the CMS barrel region [3].

A schematic picture of the ratio is shown in Figure 17. We note that the events in the numerator typically have values of $\cos\theta^*$, close to zero, so the numerator is sensitive to new physics which tends to be relatively isotropic (flat in $\cos\theta^*$). In contrast the events in the denominator typically have larger values of $\cos\theta^*$, closer to 0.7. The denominator will mainly contain background from QCD dijets, which are dominated by a t-channel scattering angular distribution roughly proportional to $1/(1-\cos\theta^*)^2$.

5.1 QCD Background

The full CMS simulation of the dijet ratio from QCD is shown in Figure 18. The dijet ratios from corrected CaloJets and from GenJets are quite similar, and the the ratio from CaloJets is shifted due to variation of the jet response versus η within the barrel. Each set of points is fit to a horizontal line and the fit value and statistical error is shown. For the old η cuts the dijet ratio from corrected CaloJets and from GenJets is flat at 0.6. It was also flat at 0.6 in the PTDR2 analysis [1, 8] up to the largest simulated mass values of 6.5 TeV, and was flat at around 0.6 in the DØ measurement, both of which used the old cuts. Figure 18 also shows that the dijet ratio for CaloJets and GenJets for the optimized eta cuts. It is flat at 0.5 for dijet masses up to about 6 TeV. Dijets with mass values above 6 TeV from QCD are expected to be seen only for integrated luminosities above 1 fb^{-1}. In summary, the simulated dijet ratio from QCD is 0.6 for the old η cuts and 0.5 for the optimized η cuts in the dijet mass region of interest.

5.2 Optimization of η cuts

We optimized the η cuts to maximize the sensitivity of the signal with respect to the background within the barrel region of the CMS calorimeter [3]. A χ^2 between the background and the signal was calculated using the expected Gaussian statistical errors on the QCD background. To have optimal sensitivity early in CMS running, we used an integrated luminosity of 100 pb^{-1} for the Gaussian errors on QCD, and a contact interaction signal of Λ^+ = 5 TeV was chosen. Both signal and background were determined with a sample of GenJets, since there was no difference

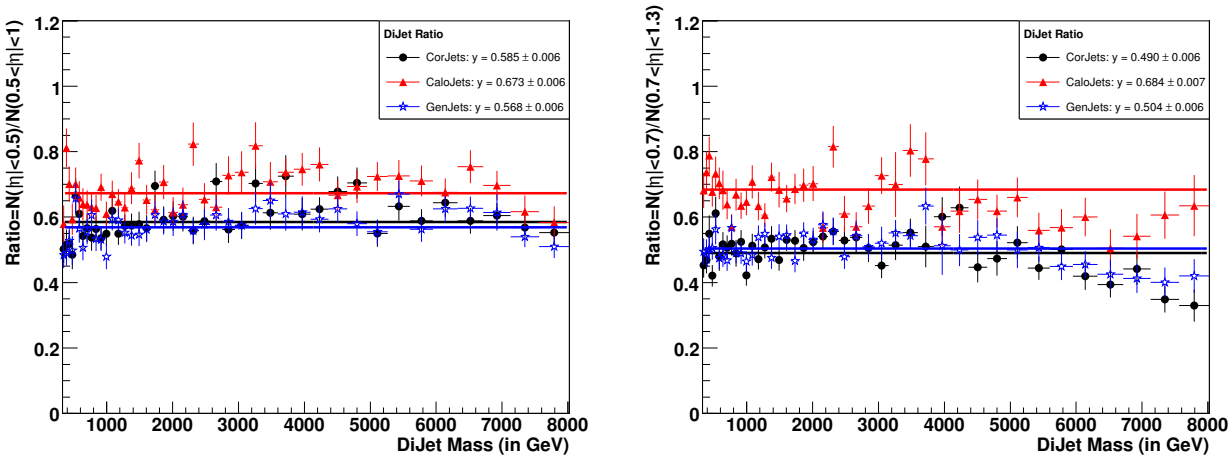

Figure 18: Simulation of dijet ratio from QCD for GenJets, CaloJets, and CorJets for the old η cuts (left) and the optimized η cuts (right).

between GenJets and CaloJets for the QCD background, and we do not expect much difference for the signal. We varied η_{in} from 0.3 to 0.9 in steps of 0.1, and η_{out} from 0.9 to 1.3 in steps of 0.1, and found the χ^2 listed in table 5. Within the barrel the χ^2 is maximum at a value of 200 for $\eta_{in} = 0.7$, $\eta_{out} = 1.3$, an order of magnitude larger than the χ^2 for the old cuts. In Fig. 19 we compare the simulated signal and QCD background fit with the old and optimized η cuts. The contact interaction signal is visibly more significant with the optimized cuts.

	0.9	1.0	1.1	1.2	1.3
0.3	4.6	9.8	19.8	32.0	44.9
0.4	7.0	16.6	34.5	56.3	80.6
0.5	9.1	20.4	55.1	91.6	128.9
0.6	9.1	21.9	63.6	129.6	182.3
0.7	4.2	13.7	54.8	116.1	199.9
0.8		12.7	50.1	101.8	170.8
0.9			35.7	86.4	145.3

Table 5: χ^2 between QCD and QCD plus a contact interaction as function of inner (first column) and outer (first row) η cuts for 100 pb^{-1} and $\Lambda = 5$ TeV.

Luminosity	10 pb^{-1}				100 pb^{-1}				1 fb^{-1}			
Λ (TeV)	3	5	10	15	3	5	10	15	3	5	10	15
χ^2 (stat)	151	5.6	0.01	0.0001	2450	169.1	0.5594	0.0054	2.83e+04	3005	22.32	0.4271

Table 6: χ^2 between QCD (background) and QCD plus a contact interaction (signal) for the optimized η cuts.

	95% CL Excluded Λ (TeV)			5σ Discovered Λ (TeV)		
	10 pb^{-1}	100 pb^{-1}	1 fb^{-1}	10 pb^{-1}	100 pb^{-1}	1 fb^{-1}
DØ and PTDR η cuts	< 3.8	< 6.8	< 12.2	< 2.8	< 4.9	< 9.1
Optimized η cuts	< 5.3	< 8.3	< 12.5	< 4.1	< 6.8	< 9.9

Table 7: Sensitivity to contact interactions with 10 pb^{-1}, 100 pb^{-1}, and 1 fb^{-1} for both the old η cuts and the optimized η cuts. Estimates include statistical uncertainties only.

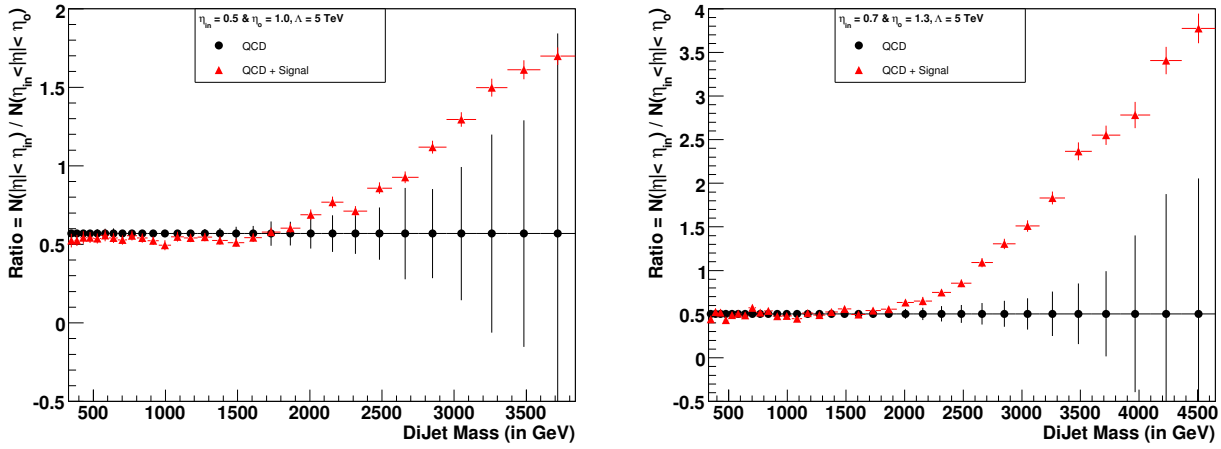

Figure 19: Dijet ratio from smoothed QCD (circles) and QCD plus a 5 TeV contact interaction (triangles) for the old η cuts from Tevatron (left plot) and for the optimized η cuts (right plot).

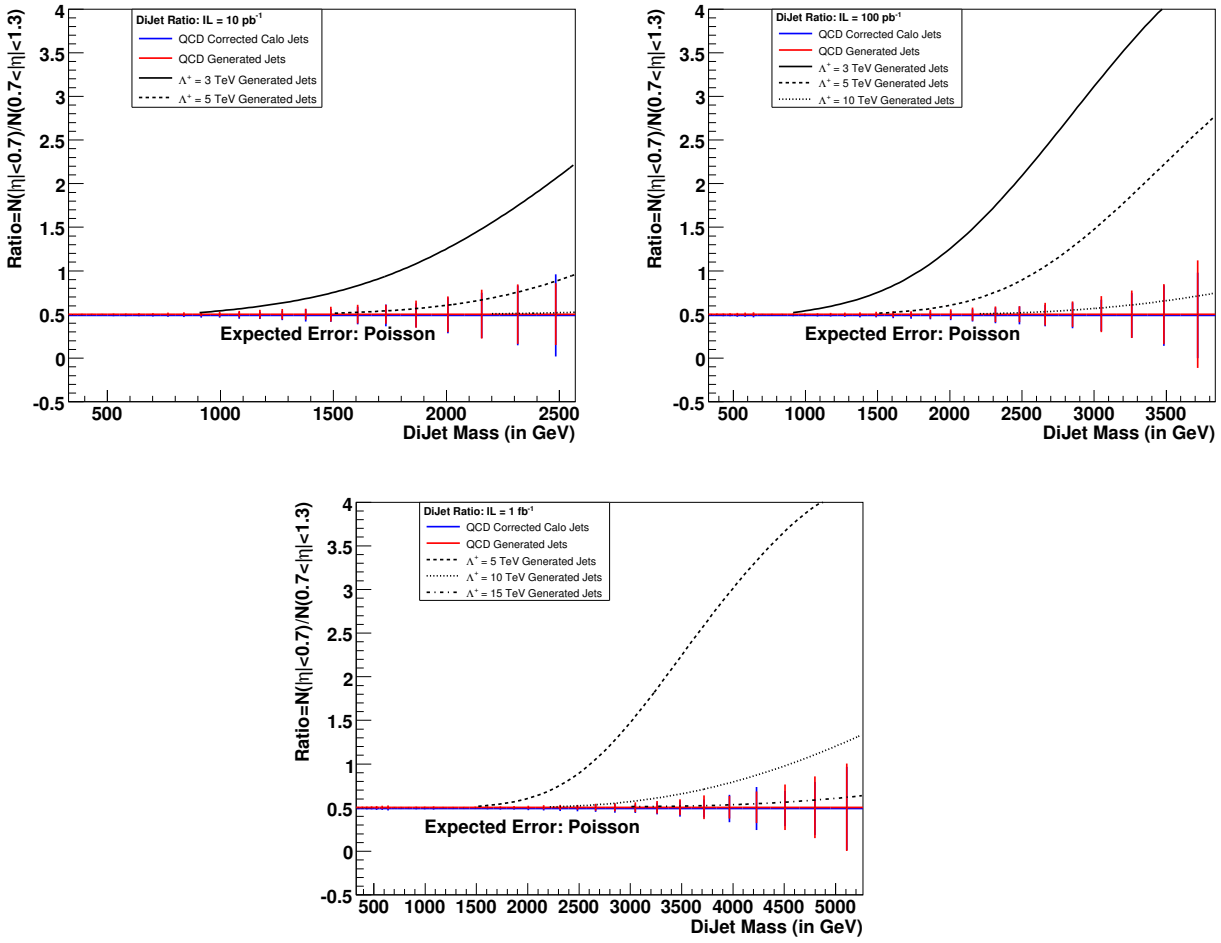

Figure 20: Dijet Ratio of QCD is compared with QCD plus a contact interaction for the optimized η cuts and four values of integrated luminosity: 10 pb^{-1} (top left), 100 pb^{-1} (top right) and 1 fb^{-1} (bottom).

5.3 Sensitivity to Contact Interactions

In Figure 20 we compare contact intact interaction signals of Λ^+ =3, 5, 10 and 15 TeV to the QCD background levels and their expected statistical uncertainty for integrated luminosities of 10 pb^{-1}, 100 pb^{-1} and 1 fb^{-1}. The

χ^2 between signal and background is listed in table 6. The scales we expect to be able to exclude at 95% CL or discover at 5σ significance are found using the χ^2 interpolation technique described in our previous analysis [8]. The resulting sensitivities are listed in table 7 for both the new optimized η cuts and the old η cuts inherited from the Tevatron. The gain in sensitivity from the new cuts at low integrated luminosity is significant. Systematic uncertainties are small because they cancel in the ratio. The affect of systematic uncertainties on our Λ sensitivity was previously found to be roughly $0.1 - 0.2$ TeV for the old η cuts [8], and we expect a similar value for the optimized η cuts. Even after including systematics we expect that with only 10 pb^{-1} CMS should be able to discover at 5σ significance a contact interaction scale $\Lambda^+ = 4$ TeV, or exclude at 95% CL a scale $\Lambda^+ = 5$ TeV, around twice the Tevatron exclusion of $\Lambda^+ < 2.7$ TeV [13].

5.4 Sensitivity to Dijet Resonances

The dijet ratio is a simple variable we can use to search for dijet resonances. In figure 2 we showed that s-channel resonances have a more isotropic decay angular distribution than QCD dominated by t-channel processes. Resonances will therefore have a larger value of the dijet ratio than QCD. In figure 21 we show the dijet ratio for dijet resonances as a function of resonance mass compared to the flat level of 0.5 expected for QCD. In this figure we used GenJets for the decays of three different resonance types, and also show that GenJets agree with CaloJets for the one resonance type for which we had a full CMS simulation (Z'). The relative size of the dijet ratio for dijet resonances can be understood from the angular distributions discussed in section 1.2.1. The dijet ratio is smallest for Z' which has an angular distribution that increases moderately with $\cos\theta^*$. The dijet ratio is larger for excited quarks which have an angular distribution that is flat in $\cos\theta^*$. The dijet ratio is largest for Randall-Sundrum gravitons which have an angular distribution from two out of three sub-processes that decreases with $\cos\theta^*$ in the region of moderate $\cos\theta^*$. The dijet ratio for dijet resonances does not stay constant with resonance mass, in contrast to dijet angular distributions for a given resonance sub-process which are the same at any resonance mass. This is because the dijet ratio is also sensitive to the boost of the resonance, and there is more boost at low resonance masses reducing the value of the dijet ratio.

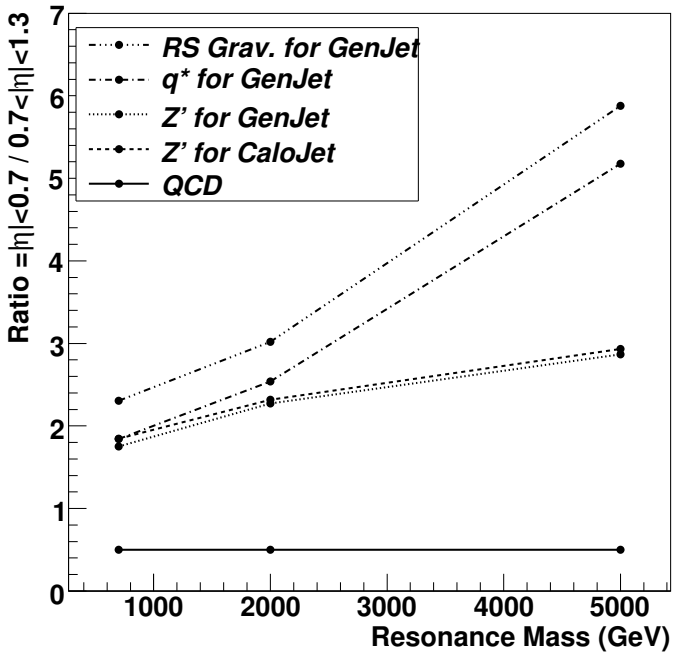

Figure 21: The dijet ratio for GenJets from decays of Randall-Sundrum gravitons, excited quarks, and Z' and for corrected CaloJets from Z' as a function of the resonance mass is compared to the dijet ratio for QCD.

The observed size of a resonance signal in the dijet ratio variable in the presence of QCD background will depend on the rate of both signal and background in both the numerator and denominator of the ratio. While the background rate is fixed by QCD, the signal rate is highly model dependent. We have chosen here to study the spin dependence of a resonance signal rate which is large enough to be observed, corresponding to an excited quark. Specifically,

we have studied signals that have the cross section for an excited quark in the region $|\eta| < 1.3$, but are allowed to have various angular distributions within $|\eta| < 1.3$ depending on the spin of the resonance. To say this another way, we consider three kinds of hypothetical resonances which are constrained to have the cross section for an excited quark:

1. Spin 1/2 resonances decaying to q g modeled by the q^* angular distribution.
2. Spin 1 resonances decaying to $q\bar{q}$ modeled by the Z' angular distribution.
3. Spin 2 resonances decaying to $q\bar{q}$ and gg modeled by the Randall-Sundrum graviton angular distribution.

and we study the effect of these spin variations at a fixed total cross section for $|\eta| < 1.3$. We do this to isolate the effect of the resonance angular distribution from that of total resonance rate. We note that this is also related more closely to an empirical measurement procedure where one might see a resonance in rate versus dijet mass, measure the total resonance rate, and then measure the dijet ratio to either determine the spin of the resonance being observed.

We note that the three cases listed above cover all the models discussed in table 1. A spin 0 dijet resonance decaying to fermions, for example an E_6 diquark, has the same isotropic angular distribution as a spin 1/2 resonance in item 1 above. Spin 1 dijet resonances decaying to fermions such as axigluons, colorons, and W' will all produce the same angular distributions as the Z' above.

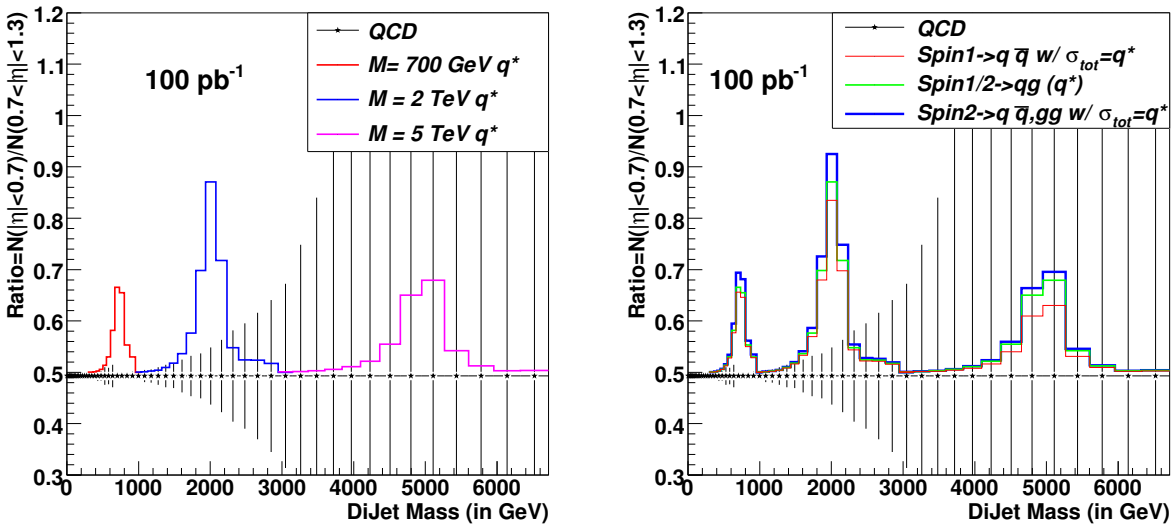

Figure 22: The diet ratio from smoothed QCD (circles) and from QCD plus a dijet resonance (histograms) is compared for an excited quark resonance hypothesis (left) and for a resonance hypothesis with the cross section of an excited quark but three different angular distributions corresponding to a spin 1/2, 1 and 2 resonance (right) for QCD error bars corresponding to an integrated luminosity of 100 pb^{-1}.

In Figure 22 we show the dijet ratio for dijet resonances in the presence of the QCD background. At dijet masses near the resonance pole mass the rate of a resonances is large enough for the resonance to be observed in the ratio variable, producing the characteristic resonance signal in the ratio variable. For an integrated luminosity of 100 pb^{-1} a convincing resonance signal is observed above the QCD statistical uncertainties for excited quarks of both 0.7 and 2 TeV. Holding the cross section of the resonance constant, and exploring the spin dependence, we see in Figure 22 that we would be able to observe a 0.7 or 2 TeV resonance with excited quark cross section for any of the three spin values 1/2, 1 or 2. In the presence of the large QCD background the signal size is not very dependent on the spin of the resonance, because they all have very similar angular distributions compared to the QCD t-channel pole which is dominating the denominator of the ratio. While it is true that the dijet ratio for the different resonance spins in Figure 21 was sometimes quite different in the absence of background, some of that difference was due to different contributions to the denominator which get overwhelmed by QCD in Figure 22. We note that if we observe a resonance in the ratio and we know its total rate, for example from the analysis in rate vs. mass from

section 4, we can use the ratio to measure the spin of the resonance. While the small spin differences in Figure 22 indicates this will be challenging, we note that the small statistical uncertainties possible with higher integrated luminosities should make it possible.

We note that the search for resonances in the djiet ratio requires very little modeling of the QCD background. Since the background is expected to be pretty flat, the resonances should be visible as bumps. We contrast this with the search for resonances in the dijet mass distribution, which is steeply falling and requires either a fit to the background or an accurate QCD prediction. Both these ways of estimating the steeply falling QCD background have issues and systematic uncertainties. In the ratio measurement this issue is avoided, because the ratio automatically divides the data into a control region (the denominator) and a signal region (the numerator), and measures the shape of the background from the control region. It is thus a promising method of discovery early in CMS running when there may be large systematic uncertainties in the shape and normalization of the QCD backround rate as a function of mass.

6 Conclusions

We have presented CMS plans to search for physics beyond the standard model using dijets, along with estimates of our sensitivity, and we reach the following conclusions which go beyond what was presented in the physics TDR.

1. We believe the CMS single jet trigger strategy is sound, and that with only small modifications in thresholds and prescales the existing single jet triggers will be optimal for dijet analysis.
2. It is important that the single jet triggers, which have a large rate, each map to a unique primary dataset that contains all events which pass that trigger threshold: for N p_T thresholds we recommend N datasets.
3. We plan to remove unwanted backgrounds from catastrophic noise, beam halo and cosmic rays by requiring each event to have MET/$\Sigma E_T < 0.3$, a cut which is fully efficient for dijets from QCD.
4. The optimal region for a dijet resonance search, $|\eta| < 1.3$, also corresponds with a region of smoothly varying response of the calorimeter, and we will measure that response using dijet balance. We recommend this cut for future analysis.
5. We have presented an improved estimate and parameterization of the dijet mass resolution. The Gaussian core of the resolution for a resonance varies from 9% at 0.7 TeV to 4.5% at 5 TeV. We recommend that this be used to form mass bins for future dijet resonance searches.
6. The following η cuts provide a new definition for the dijet ratio, $N(|\eta| < 0.7)/N(0.7 < |\eta| < 1.3)$, and are chosen to optimize our sensitivity to a contact interaction signal in early CMS running.
7. The inclusive cross section as a function of jet p_T is a first simple measure of QCD dijets from which CMS can discover a contact interaction scale $\Lambda^+ = 3$ TeV in 10 pb^{-1} of integrated luminosity.
8. With the dijet mass distribution we expect to be able to convincingly observe dijet resonances with large cross sections, such as a 2 TeV excited quark which produces at 13σ signal (statistical errors only) with 100 pb^{-1}.
9. With the dijet ratio, a simple angular measurement, we expect to be able to discover a contact interaction scale Λ^+ of 4, 7 and 10 TeV for integrated luminosities of 10 pb^{-1}, 100 pb^{-1}, and 1 fb^{-1} respectively.
10. Using the dijet ratio we can discover or confirm a dijet resonance, and eventually measure its spin. With 100 pb^{-1} a 2 TeV resonance with the production rate of an excited quark produces a convincing signal in the dijet ratio.

We hope this analysis and its conclusions will be helpful in preparing the CMS experiment to discover new physics with dijets.

References

[1] CMS Collaboration, *"CMS Physics Technical Design Report Volume II (PTDR2) : Physics Performance."*, **CERN-LHCC-2006-021; CMS-TDR-008-2; J. Phys. G: Nucl. Part. Phys. 34 995-1579**, August 2006.

[2] M. Cardaci, B. Bollen, and R. Harris, *"Dijet Resonance Analysis with CMSSW_1_2_0"*., **CMS AN-2007/016**, October 2007.

[3] M. Jha, M. Zielinski, and R. Harris, *"Dijet Ratio from QCD and Contact Interactions"*., **CMS AN-2007/015**, October 2007.

[4] K. Gumus, N. Akchurin, S. Esen and R. Harris, *"CMS Sensitivity to Dijet Resonances"*., **CMS Note 2006/070**, May 2006.

[5] B. Allanach, K. Odagiri, M. Palmer, M. Parker, A. Sabetfakhri and B. Webber, *"Exploring Small Extra Dimensions at the Large Hadron Collider"*, **JHEP 0212:039 (2002) [hep-ph/0211205]**.

[6] E. Eichten, K. Lane, and M. E. Peskin, *"New Tests for Quark and Lepton Substructure"*, **Phys. Rev. Lett. 50, 811 (1983)**.

[7] S. Esen and R. Harris, *"Jet Triggers and Dijet Mass"*., **CMS Note 2006/069**, May 2006.

[8] S. Esen and R. Harris, *"CMS Sensitivity to Quark Contact Interactions using Dijets"*., **CMS Note 2006/071**, May 2006.

[9] CDF Collaboration, F. Abe et al, *"Search for New Particles Decaying to Dijets at CDF"*, **Phys. Rev. D55: 5263-5268 (1997), hep-ex/9702004**,

[10] D. Acosta et al., *"The Underlying Event at LHC"*, **CMS-Note - 2006/067**.

[11] M. Vazquez Acosta et al., *"Jet and MET performance in CMSSW_1_2_0"*., **CMS IN-2007/053** September 2007.

[12] R. Harris, *"Jet Calibration from Dijet Balancing"*, **CMS AN 2005/034**, November 2005.

[13] B. Abbott et al., *"Dijet Mass Spectrum and a Search for Quark Compositeness in $\bar{p}p$ Collisions at $\sqrt{s} = 1.8$ TeV"*, **Phys. Rev. Lett. 82, 2457 (1999)**.